Calculation of residual stresses in injection molded products

Rheologica Acta Rheol Acta 30:284–299 (1991)

Calculation of residual stresses in injection molded products

F. P. T. Baaijens

Philips Research Laboratories, Eindhoven, The Netherlands

Abstract: Both flow- and thermally-induced residual stresses which arise during the injection molding of amorphous thermoplastic polymers are calculated in the filling and post-filling stage. To achieve this, a compressible version of the Leonov model is employed. Two techniques to calculate flow-induced residual stresses are investigated. First, a direct approach is developed where the pressure problem is formulated using the viscoelastic material model. Second, generalized Newtonian material behavior is assumed in formulating the pressure problem, and the resulting flow kinematics is used to calculate normal stresses employing the compressible Leonov model. The latter technique gives comparable results, while reducing the computational cost significantly.

Key words: Injection molding; viscoelasticity; compressible Leonov model; flow-induced residual stresses; thermally-induced residual stresses; amorphous polymers; numerical analysis

Notation and symbols

A^c conjugate of tensor A
A^d deviatoric part of A
$(\underline{\cdot})$ column
$(\underline{\cdot})^T$ transpose of a column
$(\underline{\underline{\cdot}})$ matrix
$\dot{(\cdot)}$ material time derivative
$(\cdot)_e$ elastic part of $(\cdot)$
$(\cdot)_p$ plastic part of $(\cdot)$

Symbol description

α coefficient of thermal expansion
$\dot{\gamma}$ shear rate
ε specific internal energy
λ heat conduction coefficient
θ relaxation time
η viscosity
ξ reduced time
ϱ density
v specific volume

a_T time-temperature shift factor
c_p specific heat at constant pressure
J volume change factor
N_1 first normal stress difference
p pressure
r internal heat source

$\vec{\nabla}$ gradient operator with respect to current configuration
$\vec{\nabla}_0$ gradient operator with respect to reference configuration

$\vec{h}$ heat flux
$\vec{v}$ velocity
$\vec{x}$ position vector

$\underline{\underline{\sigma}}$ Cauchy stress tensor
$\underline{\underline{\tau}}$ extra stress tensor

$\underline{\underline{D}}$ rate of strain tensor
$\underline{\underline{F}}$ deformation tensor
$\underline{\underline{B}}$ left Cauchy-Green tensor
$\underline{\underline{L}}$ velocity gradient tensor

1. Introduction

Injection molding is a commonly applied processing technology for plastics. In the past decade, attention in numerical simulations of the injection molding process has been focused on the filling stage. The key items in these calculations are the prediction of

pressure and temperature distributions and the propagation of the flow front in complex-shaped, thin-walled geometries. Numerous commercial codes are presently available, e.g., Boshouwers and v.d. Werf [1], Sitters [2], and Manzione [3].

More recently, the prediction of residual stresses (and molecular orientation) in injection molded products has attracted attention. Knowledge of residual stresses is essential to predict dimensional and shape inaccuracies of a product. Roughly, there are two sources of residual stresses. First, due to the viscoelastic nature of the polymeric melt, normal stresses develop during the filling, packing, and holding stage. Usually, these so-called flow-induced stresses are relatively small. However, they give rise to large molecular orientations which effect the mechanical and optical (birefringence) behavior of a product. They also give rise to differences in (post-) shrinkage behavior in directions perpendicular and parallel to the flow direction. The second cause of residual stresses is the rapid increase in rigidity of the material as it passes through the glass transition point (or region). Across the product wall a highly non-uniform temperature distribution exists. Consequently, each material point solidifies at a different time, leading to differential shrinkage causing thermally-induced stresses.

Initial investigations by Isayev and Hieber [4] show the potential capabilities of the so-called Leonov model, first published by Leonov [5], to predict flow-induced residual stresses during the filling stage. Birefringence measurements of Wimberger-Friedl and Janeschitz-Kriegl [13] in Compact Discs indicate that molecular orientation is introduced not only during the filling, but also during the post-filling (packing and holding) stages of the injection molding process. The traditional incompressible version of the model as applied by Isayev and Hieber [4] is slightly modified to include compressibility effects, an essential feature in the packing stage. By following Stickforth [6] and Simo [7], a kinematic split of the elastic deformation tensor into a volumetric and a deviatoric part is defined and a compressible version of the Leonov model is derived. As the model reduces to that of a linear viscoelastic medium for small deformations, only linear viscoelastic measurements are required to determine the material properties.

Two approaches to calculate flow-induced residual stresses by means of the compressible Leonov model are investigated. Firstly, the viscoelastic material behavior is taken into account to derive the so-called pressure problem (Sitters [27]); this is called the *direct* approach. Secondly, an *indirect* method is developed where the pressure problem is derived by employing a generalized Newtonian model, while the resulting flow kinematics is used as input for the viscoelastic constitutive equation to calculate flow-induced residual stresses. The latter approach considerably reduces computational time.

2. Governing equations

The three-dimensional governing equations are:

1) The continuity equation, representing the conservation of mass

$$\frac{\dot{\varrho}}{\varrho} + \vec{\nabla}\cdot\vec{v} = 0 \ , \tag{2.1}$$

where ϱ represents the density (the inverse of the specific volume v), $\vec{\nabla}$ is the gradient operator, and $\vec{v}$ the velocity field.

2) The momentum equation

$$\vec{\nabla}\cdot\boldsymbol{\sigma} + \varrho\vec{f} = \varrho\dot{\vec{v}} \ , \tag{2.2}$$

where $\boldsymbol{\sigma}$ is the Cauchy stress tensor and $\vec{f}$ is the body force per unit mass.

3) The energy equation

$$\varrho\dot{\varepsilon} = \boldsymbol{\sigma} : \boldsymbol{D} - \vec{\nabla}\cdot\vec{h} + \varrho r \ , \tag{2.3}$$

where ε is the specific internal energy, $\boldsymbol{D}$ is the rate of strain tensor, $\vec{h}$ the heat flux, and r an internal heat source.

This set of equations cannot be solved as such: constitutive equations for the density, the Cauchy stress tensor, the specific internal energy, the heat flux, and the internal heat source must be given, accompanied by appropriate initial and boundary conditions. This is the object of the next chapter.

However, some remarks can be made here. First, due to the extremely high viscosity of the material compared to the velocities, inertia effects are disregarded in the momentum equation. Body forces can be disregarded and no internal heat source is assumed to be present. Further, solving the full three-dimensional theory would be highly uneconomical, and would bypass the typical geometrical properties of the product, such as narrowness and weak curvature. With a few suitably chosen kinematical assumptions, a much more workable theory is derived.

3. Constitutive models

3.1 The compressible Leonov model

Constitutive models are given to describe the thermodynamic behavior of isotropic amorphous polymers. First, a model is presented to characterize the thermo-mechanical behavior. Thereafter, thermal properties are discussed briefly.

At mechanical excitation, amorphous polymers show both a fast, rigid glass-like response and a slow, weak liquid-like response. When analyzing the injection molding process, the liquid response dominates in the molten state, whereas the glassy response is relevant in the solidified state.

In the molten state the polymer is subjected to large deformations. The mechanical behavior in shear dominated flows (as in injection molding) can be described reasonably well with the so-called Leonov model, as shown by, e.g., Upadyay et al. [8]. During the filling stage, compressibility effects may be disregarded, as opposed to the post-filling stage, where compressibility is one of the key phenomena.

The basic kinematical assumptions of a compressible version of the Leonov model are discussed briefly. The prime assumption made by Leonov [5] is that the deformation tensor $\boldsymbol{F}$, relating the current to the reference configuration, can be decomposed multiplicatively into an elastic ($\boldsymbol{F}_e$), and a plastic ($\boldsymbol{F}_p$) part: $\boldsymbol{F} = \boldsymbol{F}_e \cdot \boldsymbol{F}_p$; see Leonov [5, 9] and Stickforth [6]. Secondly, it is assumed that the polymer cannot be given a (permanent) plastic volume change, i.e., $J_p = \det(\boldsymbol{F}_p) = 1$ and $J_e = \det(\boldsymbol{F}_e) = \det(\boldsymbol{F}) = J$. So, all volumetric changes due to external loading must be elastic in nature.

Following Simo [7], volumetric changes embedded in $\boldsymbol{F}_e$ are separated from the deviatoric responses by defining the kinematic split

$$\bar{\boldsymbol{F}}_e = J^{-1/3} \boldsymbol{F}_e \ . \tag{3.1}$$

The left Cauchy-Green strain tensors associated with $\boldsymbol{F}, \boldsymbol{F}_e$ and $\bar{\boldsymbol{F}}_e$ are

$$\boldsymbol{B} = \boldsymbol{F} \cdot \boldsymbol{F}^c \ , \quad \boldsymbol{B}_e = \boldsymbol{F}_e \cdot \boldsymbol{F}_e^c \ , \quad \bar{\boldsymbol{B}}_e = \bar{\boldsymbol{F}}_e \cdot \bar{\boldsymbol{F}}_e^c \ . \tag{3.2}$$

If $\boldsymbol{L} = (\vec{\nabla} \vec{v})^c$ is the velocity gradient tensor, then $\boldsymbol{L} = \dot{\boldsymbol{F}} \cdot \boldsymbol{F}^{-1}$. It is common practice to decompose $\boldsymbol{L}$ additively into an elastic and a plastic part:

$$\begin{aligned} &\boldsymbol{L} = \boldsymbol{L}_e + \boldsymbol{L}_p \ , \quad \boldsymbol{L}_e = \dot{\boldsymbol{F}}_e \cdot \boldsymbol{F}_e^{-1} \ , \\ &\boldsymbol{L}_p = \boldsymbol{F}_e \cdot \dot{\boldsymbol{F}}_p \cdot \boldsymbol{F}_e^{-1} \ . \end{aligned} \tag{3.3}$$

This is nothing but a definition of $\boldsymbol{L}_e$ and $\boldsymbol{L}_p$, providing a tool to include relaxation in the constitutive model. These are used to define spin ($\boldsymbol{W}_\alpha$) and deformation rate ($\boldsymbol{D}_\alpha$) tensors

$$\begin{aligned} &\boldsymbol{L}_\alpha = \boldsymbol{D}_\alpha + \boldsymbol{W}_\alpha \ , \quad \boldsymbol{D}_\alpha^c = \boldsymbol{D}_\alpha \ , \\ &\boldsymbol{W}_\alpha^c = -\boldsymbol{W}_\alpha \quad \alpha = [-], e, p \ . \end{aligned} \tag{3.4}$$

In accordance with Leonov [5], $\boldsymbol{W}_p$ is chosen equal to the null tensor: $\boldsymbol{W}_p = \boldsymbol{0}$. Finally, it can be shown that

$$\dot{\bar{\boldsymbol{B}}}_e = (\boldsymbol{L}^d - \boldsymbol{D}_p) \cdot \bar{\boldsymbol{B}}_e + \bar{\boldsymbol{B}}_e \cdot (\boldsymbol{L}^{dc} - \boldsymbol{D}_p) . \tag{3.5}$$

The Cauchy stress tensor $\boldsymbol{\sigma}$ is split into an elastic part ($\boldsymbol{\sigma}_e$), and a plastic part ($\boldsymbol{\sigma}_p$): $\boldsymbol{\sigma} = \boldsymbol{\sigma}_e + \boldsymbol{\sigma}_p$. First the elastic stresses are defined, then the plastic part is given. Thereafter the temperature dependence of the material parameters is discussed, and finally the linearized model is given.

Elastic stresses: It is common practice to decompose $\boldsymbol{\sigma}_e$ into a hydrostatic and a deviatoric part: $\boldsymbol{\sigma}_e = -p\boldsymbol{I} + \boldsymbol{\tau}^e$. In the single mode case $\boldsymbol{\tau}^e$, is chosen as $\boldsymbol{\tau}^e = \frac{\eta}{\theta} \bar{\boldsymbol{B}}_e^d$. However, such a choice gives poor correspondence with experimental data. Therefore, the following extension to the multi-mode case is generally proposed. The elastic extra stress tensor $\boldsymbol{\tau}^e$ is chosen as

$$\boldsymbol{\tau}^e = \sum_{k=1}^{n} \frac{\eta_k}{\theta_k} \bar{\boldsymbol{B}}_{ek}^d \ . \tag{3.6}$$

For each mode k, the unimodular left Cauchy-Green tensor $\bar{\boldsymbol{B}}_{ek}$ is calculated from (3.5), hence a relation for $\boldsymbol{D}_{pk}$ needs to be given. By analogy with Leonov's [5] proposal, the following form is chosen:

$$\boldsymbol{D}_{pk} = \frac{1}{4\theta_k} (\bar{\boldsymbol{B}}_{ek}^d - \bar{\boldsymbol{B}}_{ek}^{-d}) \ . \tag{3.7}$$

Substitution of (3.7) into (3.5) yields for each mode k

$$\begin{aligned} \dot{\bar{\boldsymbol{B}}}_{ek} = {} & \boldsymbol{L}^d \cdot \bar{\boldsymbol{B}}_{ek} + \bar{\boldsymbol{B}}_{ek} \cdot \boldsymbol{L}^{dc} - \frac{1}{2\theta_k} \\ & \times (\bar{\boldsymbol{B}}_{ek} \cdot \bar{\boldsymbol{B}}_{ek} - \boldsymbol{I} - \frac{1}{3} (\operatorname{tr}(\bar{\boldsymbol{B}}_{ek}) - \operatorname{tr}(\bar{\boldsymbol{B}}_{ek}^{-1})) \bar{\boldsymbol{B}}_{ek}) \ . \end{aligned} \tag{3.8}$$

This expression is nothing but a definition of $\bar{\boldsymbol{B}}_{ek}$. Note that, in contrast with the incompressible Leonov model, for plane flow $\operatorname{tr}(\bar{\boldsymbol{B}}_{ek}) \neq \operatorname{tr}(\bar{\boldsymbol{B}}_{ek}^{-1})$.

A relation for the pressure p remains to be given. This is done implicitly by taking a suitable relation for the specific volume. The so-called Tait equation is a successful model for amorphous polymers (Zoller, [10]) and is given by

$$v(p,T) = (a_0 + a_1(T - T_g)) \times \left(1 - 0.0894 \ln\left(1 + \frac{p}{B}\right)\right) , \tag{3.9}$$

where T_g is the pressure-dependent glass transition temperature, i.e., $T_g(p) = T_g(0) + sp$, and $B(T) = B_0 \exp(-B_1 T)$.

Plastic stresses: The plastic part of σ is chosen as

$$\sigma_p = 2\eta'(T,p)\boldsymbol{D}^d . \tag{3.10}$$

Time-temperature superposition: Thermorheologically simple behavior is assumed, implying that

$$\eta_k = a_T(T)\eta_{k0} , \quad \theta_k = a_T(T)\theta_{k0} , \quad \eta' = a_T(T)\eta'_0 , \tag{3.11}$$

where a_T is the shift factor and η_{k0} and θ_{k0} are the viscosity and relaxation time at a reference temperature, say T_0. The shift factor is governed by the WLF equation if $T \geq T_g$, i.e.,

$$\log a_T(T) = \frac{C_1(T - T_0)}{C_2 + T - T_0} , \tag{3.12}$$

while, below T_g

$$a_T(T) = a_T(T_g) . \tag{3.13}$$

The reason for this last choice is that below T_g, relaxation processes are extremely slow and hence take place at a time scale beyond current interest.

Linearized model: In the solidified state, deformations and rotations are small. In that case the above model reduces to a linear Maxwell model. Hence,

$$\boldsymbol{\tau}^e = \sum_{k=1}^{n} \boldsymbol{\tau}_k^e , \quad \boldsymbol{\tau}_k^e = \int_0^t 2\frac{\eta_{k0}}{\theta_{k0}} e^{-(\xi_{tk} - \xi_{sk})} \boldsymbol{D}^d(s)\, ds , \tag{3.14}$$

where

$$\xi_{qk} = \int_0^q \frac{1}{a_T(s)\theta_k} ds , \quad q = t, s . \tag{3.15}$$

By linearizing $\dot{v} = v \operatorname{tr}(\boldsymbol{D})$ an explicit relation for the pressure p can be derived:

$$p(t) = \int_0^t (\beta \dot{T} - \kappa \operatorname{tr}(\boldsymbol{D}))\, ds , \tag{3.16}$$

where

$$\beta = \alpha\kappa , \quad \alpha = \frac{1}{v}\left(\frac{\partial v}{\partial T}\right) \quad \text{and} \quad \frac{1}{\kappa} = -\frac{1}{v}\left(\frac{\partial v}{\partial p}\right) . \tag{3.17}$$

3.2 Thermal behavior

To calculate the temperature distribution in the polymer, constitutive equations for the heat flux and the specific internal energy are given.

Heat flux: The heat flux vector $\vec{h}$ is assumed to obey Fourier's law, that is

$$\vec{h} = -\lambda \vec{\nabla} T . \tag{3.18}$$

Specific internal energy: If elastic effects upon the specific internal energy are disregarded it can be shown that (Sitters [2])

$$\dot{\varepsilon} = c_p \dot{T} - pv \operatorname{tr}(\boldsymbol{D}) + \frac{T}{\varrho^2}\frac{\partial \varrho}{\partial T}\dot{p} , \tag{3.19}$$

where c_p is the specific heat at constant pressure.

4. Injection molding theory

4.1 Introduction

In this section the set of balance equations and constitutive equations of the previous sections are simplified considerably by introducing a number of geometrical assumptions. Only narrow, weakly curved cavities are considered such that the thin film approximation holds (see Fig. 1). For generalized Newtonian material behavior this procedure is well described in, e.g., Sitters [2]. Here a viscoelastic material model is used.

The concept of generalized Newtonian flow only holds for fully-developed flow situations. However, fully developed flow never occurs during injection molding. Yet, generalized Newtonian material behavior may be a good approximation in core regions, sufficiently far departed from sudden geometry changes (i.e., contractions) and the flow front, while the temperature needs to be sufficiently high.

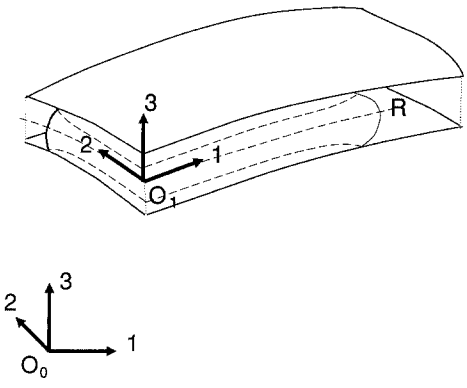

Fig. 1. Definition of the local basis O_1

Near the solidified layers fully-developed flow is unlikely to occur, since relaxation processes slow down considerably as the temperature approaches the glass transition temperature. During post-filling the temperature drops in the entire channel. So, it may be expected that viscoelastic phenomena do affect the filling and post-filling stages.

Incidentally, viscoelastic phenomena are definitely present at the gate where enormous elongational effects take place. However, elongational flow is not considered in the lubrication theory. This is a serious shortcoming of most mold-filling analysis programs, because the overall pressure drop may be largely affected by the elongational effects at the gate. The solution to this problem is beyond the scope of this paper.

The mechanical and thermal description of the solid state is quite different from that of the molten state. A simple and effective membrane type of structural mechanics theory is used to describe the development of thermally-induced residual stresses.

In the liquid state the compressible Leonov model is used, with a set of n relaxation times (θ_k) and viscosities (η_k). In the solid state the linearized version, the generalized Maxwell model is used, with another set of m relaxation times ($\bar{\theta}_k$) and viscosities ($\bar{\eta}_k$).

Preliminaries: At each point $\vec{x}_R$ of the midplane R, a local orthonormal basis $O_1 = \{\vec{e}_1, \vec{e}_2, \vec{e}_3\}$ can be defined, such that $\vec{e}_1$ and $\vec{e}_2$ are tangential to R, and $\vec{e}_3$ is normal to R, e.g., $\vec{e}_3 = \vec{n}$. As a global orthonormal basis $O_0 = \{\vec{e}_1^0, \vec{e}_2^0, \vec{e}_3^0\}$ is defined. To transform quantities with respect to O_0 to O_1, the rotation matrix $\underline{Q}$ is defined as $Q_{ij} = \vec{e}_j \cdot \vec{e}_i^0$. Let $\vec{x}_R$ identify a particle at the midplane R. The position vector of a particle along $\vec{n}$ that emanates from $\vec{x}_R$ is denoted by $\vec{x}$. Now, let A be an arbitrary second order tensor and $\vec{a}$ some vector, then the components of A, respectively $\vec{a}$, with respect to O_1 follow from $A_{ij} = A : \vec{e}_j \vec{e}_i$, and $a_i = \vec{a} \cdot \vec{e}_i$, respectively, with $i = 1,2,3$.

The channel height is denoted by h_m, and the current product wall thickness by h_c.

4.2 Flow-induced residual stresses

Assumptions:

1) With respects to O_1, it is assumed that the contribution of the normal stresses can be disregarded in the momentum equation. This can be made plausible by noting that gradients in the thickness direction are far superior to the in-plane gradients.
2) The pressure is independent of the $\vec{e}_3$ direction.
3) The material is assumed to flow into the domain with a fully developed velocity profile.
4) Fountain phenomena are not considered.
5) Thermal conduction tangential to the midplane R is disregarded.

Due to these assumptions, the momentum equation is approximated by (with respect to O_1)

$$\nabla p = \frac{\partial}{\partial x_3} \underline{\tau} \ , \tag{4.1}$$

$$p = p(x_1, x_2) \ , \tag{4.2}$$

with

$$\nabla^T = \left[\frac{\partial}{\partial x_1} \ \frac{\partial}{\partial x_2} \right] \text{ and } \underline{\tau}^T = [\tau_{13} \ \tau_{23}] \ . \tag{4.3}$$

The above approximation is often referred to as the thin film or lubrication theory. Employing the viscoelastic model (3.6), it follows from $\boldsymbol{\sigma} = \boldsymbol{\sigma}_e + \boldsymbol{\sigma}_p$, $\boldsymbol{\sigma}_e = -p\boldsymbol{I} + \boldsymbol{\tau}_e$ and (3.10) that

$$\tau_{i3} = \eta' \frac{\partial v_i}{\partial x_3} + \tau_{i3}^e \ , \quad \tau_{i3}^e = \sum_{k=1}^{n} \frac{\eta_k}{\theta_k} \bar{\boldsymbol{B}}_{ek}^d : \vec{e}_3 \vec{e}_i \ ,$$
$$i = 1,2 \ . \tag{4.4}$$

With respect to O_1, the continuity equation (2.1) is written as

$$\nabla^T \underline{v} + \frac{\partial v_3}{\partial x_3} = -\frac{\dot{\varrho}}{\varrho} \ , \quad \underline{v}^T = [v_1 \ v_2] \ . \tag{4.5}$$

From this the so-called pressure problem can be derived (see Appendix):

PE Given $T(\vec{x},t)$, find $p(x_1,x_2,t)\geq 0$ such that

$$\underline{\nabla}^T(S\underline{\nabla}p+\hat{\underline{\tau}}) = -\int_{s^-}^{s^+}\frac{\dot{\varrho}}{\varrho}dx_3-\frac{dh}{dt}\ ,\quad p\geq 0\ , \tag{4.6}$$

$$S = -J_2+\frac{J_1^2}{J_0}\ ,\quad J_i=\int_{s^-}^{s^+}\frac{x_3^i}{\eta'}dx_3\ ,\quad i=0,1,2\ , \tag{4.7}$$

$$\hat{\underline{\tau}}^T = [\hat{\tau}_{13}\ \hat{\tau}_{23}]\ ,$$

$$\hat{\tau}_{i3} = -\frac{J_1}{J_0}\int_{s^-}^{s^+}\frac{\tau_{i3}^e}{\eta'}dx_3+\int_{s^-}^{s^+}\frac{x_3\tau_{i3}^e}{\eta'}dx_3\ ,$$

$$i=1,2\ . \tag{4.8}$$

In this, S is the so-called fluidity coefficient, and s^+ and s^- denote the locations of the solidified layers. In addition, $\hat{\underline{\tau}}$ represents the contribution of elastic effects, $\int_{s^-}^{s^+}\dot{\varrho}/\varrho\ dx_3$ represents compressibility, and dh/dt accounts for mold elasticity. Note that for symmetric flow $J_1=0$. The pressure p is not allowed to drop below zero, because as soon as p becomes zero the material loses contact with the mold. Obviously, boundary conditions need to be introduced in the definition of **PE**, however, they are identical to the Newtonian case and can be found in, e.g., Sitters [2], they are briefly summarized here. At the gate either the flow rate or the pressure is prescribed. The pressure is assumed negligible at the flow front and no fluid may penetrate the solid walls of the mold.

Equation (4.6) is taken as a starting point for the finite element implementation. Various aspects of this implementation can be found in, e.g., Sitters [2].

Problem **PE** defines the *direct* method, in the sense that viscoelastic material behavior is assumed at the onset of deriving the pressure problem. In the *indirect* method **PE** is simplified substantially by assuming generalized Newtonian material behavior. In that case, $\hat{\underline{\tau}}=\underline{0}$, and the viscosity η' is replaced by the steady state viscosity of the incompressible Leonov model [5], see Section 4.4, Eq. (4.33). The resulting flow kinematics (velocity and shear rate field) are supplied to the viscoelastic constitutive equation to calculate (as a post-processing step) flow-induced residual stresses, giving remarkably good results, even in the post-filling stage.

4.3 Thermally-induced residual stresses

Thermally-induced residual stresses develop in the solidified layers. In this section the linearized model (3.14)–(3.17) is reduced by taking a number of kinematic and dynamic assumptions into account. The reduced constitutive equation is then embedded in a membrane type of finite element.

Assumptions:

1) Displacements and rotations are small.
2) Bending is unimportant. This is reasonable because the in-plane deformations are small, the channel is only weakly curved and the out-of-plane displacements are severely restricted by the mold. Yet, as soon as the product is ejected from the mold bending is one of the key phenomena.
3) The displacement field $\vec{u}$ is homogeneous in the normal direction, e.g.,

$$\vec{u}(\vec{x}) = \vec{u}(\vec{x}_R)\ . \tag{4.9}$$

So, if the solidified layers are separated by fluid, they both displace in the same manner: they are virtually coupled to each other.

4) Due to the presence of the mold, all normal displacements are assumed to be suppressed:

$$\vec{u}(\vec{x}_R)\cdot\vec{n} = 0. \tag{4.10}$$

In fact, due to shrinkage a small clearance between product and mold may develop and hence small lateral displacements may occur. Yet, these are sufficiently small to be disregarded in a first approximation.

5) With respect to O_1, the shear strains ε_{13} and ε_{23} are disregarded.
6) The normal stress σ_{33} is homogeneous in the normal direction.
7) As long as $\sigma_{33}<0$ the material sticks to the mold.
8) Solidification takes place at the glass-transition temperature, and flow-induced stresses do not relax after solidification. The flow-induced stress upon solidification is denoted τ_{ve}.
9) Mold elasticity is disregarded, i.e., $dh/dt=0$.

Reduced constitutive equation: Since displacements in the solidified material are small, the linearized constitutive model (3.14)–(3.17) can be used. Assume that at $t=t_n$ the stress state is known. Consider the state transition $t_n\rightarrow t_{n+1}, t_{n+1}-t_n=\Delta t$. During this transition it is assumed that $\dot{T}$ and $\boldsymbol{D}$ are constant. Let

$\Delta T = \dot{T}(t_{n+1})\Delta t$ and $\varepsilon = D\Delta t$. The Cauchy stress tensor at $t = t_{n+1}, \sigma^{n+1}$, satisfies

$$\sigma^{n+1} = \tilde{\sigma} + \tilde{\kappa}\,\mathrm{tr}\,(\varepsilon) I + 2\tilde{G}\varepsilon^d \ , \tag{4.11}$$

with

$$\tilde{\sigma} = -p_s(t_n) I + \sum_{k=1}^{m} e^{-\xi_{\Delta tk}} \tau_k(t_n) - \tilde{\beta}\Delta T I + \tau_{ve} \ , \tag{4.12}$$

$$\xi_{\Delta tk} = \int_{t_n}^{t_n+\Delta t} \frac{1}{a_T(s)\bar{\theta}_k} ds \ , \tag{4.13}$$

$$\tilde{\beta} = \frac{1}{\Delta t}\int_{t_n}^{t_{n+1}} \beta\, ds \ , \quad \tilde{\kappa} = \frac{1}{\Delta t}\int_{t_n}^{t_{n+1}} \kappa\, ds \ ,$$

$$\tilde{G} = \sum_{k=1}^{m} \frac{1}{\Delta t}\int_{t_n}^{t_{n+1}} \frac{\bar{\eta}_{k0}}{\bar{\theta}_{k0}} e^{-(\xi_{t_{n+1}k} - \xi_{sk})} ds \ , \tag{4.14}$$

where p_s denotes the hydrostatic pressure in the solid state, as opposed to the pressure in the melt p. Let at $t = t_g$ solidification take place, then $\sigma(t_g) = -p(t_g)I + \tau_{ve}(t_g)$. So, the above updating scheme for σ holds for $t > t_g$. The constitutive equation (4.11) can be simplified considerably. Due to assumptions 6 and 7, the normal stress σ_{33} can be determined by distinguishing between the situation where a fluid still exists and the situation where all the fluid has solidified in the x_3-direction.

Remark 4.1: The choice $\sigma(t_g) = -p(t_g)I + \tau_{ve}(t_g)$ is controversial. It is not clear to what extent flow-induced residual stresses actually contribute to the stress state at temperatures significantly below the glass transition temperature. The existence of normal stresses in a polymer melt is attributed to the molecule's ability to regain its most preferred, unoriented, state. This is only possible at sufficiently high temperatures. Therefore the above choice of $\sigma(t_g)$ is questionable, and an alternative seems to be: $\sigma(t_g) = -p(t_g)I$. This last definition is used in practical calculations later on. However, as $\tau_{ve}(t_g)$ is very small compared to the final stress state at room temperature, the actual difference between the two alternatives is very small.

If a fluid phase still exists, then σ_{33} is obviously equal to the pressure in the melt

$$\sigma_{33} = -p \ . \tag{4.15}$$

Note that $p \geq 0$.

If all the material has solidified in the normal direction, then the material may either stick to the walls or move tangential to the midplane R. If it sticks to the walls then $\varepsilon_{11} = \varepsilon_{22} = 0$ and (due to assumption 3 and 9) $\int_{-h_m/2}^{h_m/2} \varepsilon_{33}\, dx_3 = 0$; so

$$\sigma_{33} = \frac{\int_{-h_m/2}^{h_m/2} \tilde{\sigma}_{33} \dfrac{3}{4\tilde{G} + 3\tilde{\kappa}} dx_3}{\int_{-h_m/2}^{h_m/2} \dfrac{3}{4\tilde{G} + 3\tilde{\kappa}} dx_3} \ , \tag{4.16}$$

otherwise $\sigma_{33} = 0$.

In the above it is crucial to know whether or not the material still contacts the mold. The contact conditions are formulated as follows

$$h_m - h_c \leq 0 \ , \quad \sigma_{33} \leq 0 \ , \quad (h_m - h_c)\sigma_{33} = 0 \ . \tag{4.17}$$

If either of the first two conditions is violated during the solution process, the material still contacts the mold, whereas the third condition signifies that if and only if $h_m - h_c = 0$ the normal stress σ_{33} may be less than zero and vice versa.

Finally, due to assumption 5 and the knowledge of $\sigma_{33}, \varepsilon_{33}$ can be eliminated from (4.11), resulting in

$$\underset{\sim}{\sigma}^{n+1} = \underset{\sim}{M}\underset{\sim}{\varepsilon} + \underset{\sim}{g} \ , \tag{4.18}$$

where

$$\underset{\sim}{\sigma}^T = [\sigma_{11} \quad \sigma_{22} \quad \sigma_{12}] \ , \tag{4.19}$$

$$\underset{\sim}{\varepsilon}^T = [\varepsilon_{11} \quad \varepsilon_{22} \quad 2\varepsilon_{12}] \ , \tag{4.20}$$

$$\underset{\sim}{M} = \begin{bmatrix} \bar{a} & \bar{b} & 0 \\ \bar{b} & \bar{a} & 0 \\ 0 & 0 & \tilde{G} \end{bmatrix} \ , \tag{4.21}$$

$$\underset{\sim}{g} = \begin{bmatrix} \tilde{\sigma}_{11} + b/a\,(\sigma_{33} - \tilde{\sigma}_{33}) \\ \tilde{\sigma}_{22} + b/a\,(\sigma_{33} - \tilde{\sigma}_{33}) \\ \tilde{\sigma}_{12} \end{bmatrix} \ , \tag{4.22}$$

and

$$\bar{a} = a - \frac{b^2}{a} \ , \quad \bar{b} = b - \frac{b^2}{a} \ , \quad a = \frac{4\tilde{G} + 3\tilde{\kappa}}{3} \ ,$$

$$b = \frac{-2\tilde{G} + 3\tilde{\kappa}}{3} \ . \tag{4.23}$$

The definition of a and b may seem rather ad hoc, but they appear quite naturally when (4.11) is written in a form like (4.18).

Membrane element: At a certain time, say $t = t_n$ the displacement field $\vec{u}(\vec{x}_R, t_n)$ and the stress field $\sigma(\vec{x}, t_n)$ are assumed to be known. During the state transition $t_n \rightarrow t_{n+1}$, the displacement field changes with $\Delta\vec{u}$ and it is determined by employing the finite element method with bi-linear quadrilateral membrane elements.

Let the physical membrane domain be mapped on the unit cube by means of the local coordinates ξ, η and ζ such that $\xi, \eta, \zeta \in [-1, 1]$. The geometry and the displacement field are interpolated as

$$\vec{x} = \sum_{a=1}^{4} N_a(\xi, \eta)\vec{x}_a \ , \tag{4.24}$$

$$\Delta\vec{u} = \sum_{a=1}^{4} N_a(\xi, \eta)\Delta\vec{u}_a \ . \tag{4.25}$$

The strain-displacement matrix, see Hughes [14], is defined as

$$\underset{\sim}{B} = [\underset{\sim}{B}_1 \ldots \underset{\sim}{B}_4] \ , \tag{4.26}$$

with

$$\underset{\sim}{B}_a = \begin{bmatrix} B_1 & 0 & 0 \\ 0 & B_2 & 0 \\ B_2 & B_1 & 0 \end{bmatrix}, \ B_i = \frac{\partial N_a}{\partial x_i} = Q_{ij}\frac{\partial N_a}{\partial x_j^0} \ . \tag{4.27}$$

As such $\underset{\sim}{B}$ is arranged to be compatible with $\underset{\sim}{\varepsilon}$ in the sense that

$$\underset{\sim}{\varepsilon} = \underset{\sim}{B}\Delta\underset{\sim}{u} \ , \quad \Delta\underset{\sim}{u}^T = [\Delta\underset{\sim}{u}_1^T \ldots \Delta\underset{\sim}{u}_4^T] \ , \tag{4.28}$$

where $\Delta\underset{\sim}{u}_a$ contains the components of $\Delta\vec{u}$ at node a with respect to the local basis O_1.

The element stiffness matrix $\underset{\sim}{K}^e$ and the element force vector $\underset{\sim}{f}^e$ are given by

$$\underset{\sim}{K}^e = [\underset{\sim}{K}_{ab}] \ , \quad \underset{\sim}{f}^e = [\underset{\sim}{f}_a] \ , \quad a, b = 1, \ldots, 4 \ , \tag{4.29}$$

where

$$\underset{\sim}{K}_{ab} = \int_A \underset{\sim}{Q}_a^T \underset{\sim}{B}_a^T \hat{\underset{\sim}{M}} \underset{\sim}{B}_b \underset{\sim}{Q}_b \, dA \ , \tag{4.30}$$

$$\underset{\sim}{f}_a = \int_A \underset{\sim}{Q}_a^T \underset{\sim}{B}_a^T \hat{\underset{\sim}{g}} \, dA \ , \tag{4.31}$$

where A represents the area of the midplane of the element. The definition of the material matrix $\hat{\underset{\sim}{M}}$ and the initial stress column $\hat{\underset{\sim}{g}}$ depends on whether or not the material contacts the mold. If the material contacts the mold, then

$$\hat{\underset{\sim}{M}} = \int_{-h_m/2}^{s^-} \underset{\sim}{M} dx_3 + \int_{s^+}^{h_m/2} \underset{\sim}{M} \, dx_3 \ ,$$

$$\hat{\underset{\sim}{g}} = \int_{-h_m/2}^{s^-} \underset{\sim}{g} \, dx_3 + \int_{s^+}^{h_m/2} \underset{\sim}{g} \, dx_3 \ , \tag{4.32}$$

while otherwise the integration takes place over the entire material thickness, e.g., from $-h_m/2$ to $h_m/2$.

Remark 4.2: Formally, the integration from $-h_m/2$ to $h_m/2$ is inconsistent with assumptions made before. The linearized model is intended to the applied in the solid state only, whereas in the molten state the non-linear model should be applied. However, in practical situations deformations and deformation rates are small as soon as the material loses contact with the mold, since in that case most of the material has solidified already. That means that in the melt the extra-stress contribution to the Cauchy stress tensor is negligible, no matter what model is applied. Note that in the melt rigidity is very low, and high strain rates are needed to cause substantial stress development. The shrinkage of the melt, however, needs to be accounted for; integrating over the entire height is merely a way to do this.

Remark 4.3: Note that as long as the material sticks to the wall, $\underset{\sim}{\sigma}^{n+1}$ can be calculated directly from (4.18) as $\underset{\sim}{\varepsilon} = \underset{\sim}{0}$ due to assumption 7. If frictional sliding between polymer and mold is allowed, this no longer holds.

Remark 4.4: The constraint $\Delta\vec{u}\cdot\vec{n} = 0$ can be taken into account by a penalty function method. That is, the following term is added to the stiffness matrix (4.30): $\int_A \varepsilon N_a \underset{\sim}{n}\underset{\sim}{n}^T N_b dA$, where $\underset{\sim}{n}^T = [\vec{n}\cdot\vec{e}_1^0 \quad \vec{n}\cdot\vec{e}_2^0 \quad \vec{n}\cdot\vec{e}_3^0]$, and ε a sufficiently large penalty parameter.

4.4 Temperature equation

With use of (3.18) and (3.19), the energy equation (2.3) is written as

$$\varrho c_p \dot{T} = \vec{\nabla}\cdot\lambda\vec{\nabla}T + \boldsymbol{\tau} : \boldsymbol{D}^d - \frac{T}{\varrho}\frac{\partial\varrho}{\partial T}\dot{p} \ . \tag{4.33}$$

To take dissipation into account without having to deal with viscoelastic phenomena, τ in (4.9) is taken to represent the generalized Newtonian behavior of the material. Hence $\tau = 2\bar{\eta}(\dot{\gamma}, T)\boldsymbol{D}^d$, where $\dot{\gamma}$ is the shear rate ($\dot{\gamma} = \sqrt{2\boldsymbol{D}^d : \boldsymbol{D}^d}$). The viscosity $\bar{\eta}$ is obtained from the steady state behavior of the incompressible Leonov model [5] at simple shear

$$\bar{\eta}(\dot{\gamma}, T) = \eta' + \sum_{k=1}^{n} \frac{2\eta_k}{1+x_k} ,$$

$$x_k = \sqrt{(1+4\dot{\gamma}^2\theta_k^2)} . \tag{4.33}$$

Further, the conduction along the channel is disregarded due to the thinness of the cavity compared to its length. Hence with respect to O_1, the temperature problem to be solved is

PT Given $\vec{v}(\vec{x}, t)$ and $p(x_1, x_2, t)$, find $T(\vec{x}, t)$ such that

$$\varrho c_p \dot{T} = \frac{\partial}{\partial x_3}\left(\lambda \frac{\partial T}{\partial x_3}\right) + \bar{\eta}\dot{\gamma}^2 - \frac{T}{\varrho}\frac{\partial \varrho}{\partial T}\dot{p} . \tag{4.34}$$

During the filling stage the contact temperature is prescribed at the product mold interface, thereafter the mold temperature is prescribed as a boundary condition. Obviously, a much better way to obtain the temperature boundary conditions is to simultaneously calculate the temperature distribution in the mold and product throughout the process, yet this is beyond the scope of this paper.

5. Computational aspects

In all cases the implicit Euler scheme is used for temporal discretization. At each time step, first the temperature and pressure equation are solved independently, where coupling is enforced by the iterative scheme. That is, the sequence of problems to be solved at each time step is: **PT**→**PE**→**PT**→**PE**→... until convergence. The pressure problem **PE** is solved by employing the finite element method (FEM) with linear elements. The non-linearity of the resulting set of equations is dealt with in this section. The temperature problem **PT** is solved with a finite difference (FD) scheme where the differential grid is centered at each element. Four computational aspects are dealt with in more detail: the solution of the pressure problem **PE**, the method of characteristics to handle the material derivatives, the calculation of the shear rate in case of viscoelastic material behavior, and the calculation of $\bar{\boldsymbol{B}}_{ek}$.

Solution of the pressure problem: The system of Eqs. (4.6) is highly non-linear and is solved with a two-step procedure. A fully implicit scheme is used in the time domain.

Step 1. An initial estimate for the pressure p, and associated properties such as velocity and shear rate fields, are found by solving for generalized Newtonian material behavior. The viscosity is taken as the steady state viscosity of the incompressible Leonov model. Then **PE** reduces to

PV Given $T(\vec{x}, t)$, find $p(x_1, x_2, t) \geq 0$ such that

$$\nabla^T(\bar{S}\nabla p) = -\int_{s^-}^{s^+} \frac{\dot{\varrho}}{\varrho} dx_3 - \frac{dh}{dt} , \quad p \geq 0 , \tag{5.1}$$

$$\bar{S} = -\bar{J}_2 + \frac{\bar{J}_1^2}{\bar{J}_0} , \quad \bar{J}_i = \int_{s^-}^{s^+} \frac{x_3^i}{\bar{\eta}} dx_3 , \quad i = 0,1,2 . \tag{5.2}$$

Equation (5.1) is solved with a Picard iteration scheme, assuming $dh/dt = 0$

$$\int_{s^-}^{s^+} \left(\frac{1}{\varrho}\frac{\partial \varrho}{\partial p}\right)^i dx_3 \dot{p}^{i+1} + \nabla^T(\bar{S}^i \nabla p^{i+1}) = -\int_{s^-}^{s^+} \left(\frac{\dot{\varrho}}{\varrho}\right)^i dx_3 + \int_{s^-}^{s^+} \left(\frac{1}{\varrho}\frac{\partial \varrho}{\partial p}\right)^i dx_3 \dot{p}^i , \tag{5.3}$$

$$\bar{S}^i = -\bar{J}_2^i + \frac{\bar{J}_1^{2i}}{\bar{J}_2^i} , \quad \bar{J}_j^i = \int_{s^-}^{s^+} \frac{x_3^j}{\bar{\eta}^i} dx_3 , \quad j = 0,1,2 , \tag{5.4}$$

where the superscripts i and $i+1$ respectively refer to the previous or the current iteration.

Step 2. Given an estimate of the pressure, shear rate field, etc., by step *1*, **PE** is finally solved with the Newton iteration process. Within the finite element context, the element stiffness matrices are determined by numerical differentiation.

Method of characteristics: (Pironneau [11] and Morton et al. [12]). Consider the time interval $t \in [t_n, t_{n+1}]$, and let $\Delta t = t_{n+1} - t_n$. The time derivative $\dot{p}$ is approximated by

$$\dot{p} = \frac{p(\vec{x}, t_{n+1}) - p(\vec{s}_n, t_n)}{\Delta t} , \tag{5.5}$$

where $\vec{s}_n$ designates the position at time t_n of the material particle currently located at $\vec{x}$. The material time derivatives of T and $\bar{\boldsymbol{B}}_{ek}$ are treated likewise.

Calculation of the shear rate: To calculate $\bar{\boldsymbol{B}}_{ek}$, the shear rate must be known. Equation (A.2) constitutes a non-linear relation for the shear rate. It is solved pointwise with a secant-method, such that $\bar{\boldsymbol{B}}_{ek}$ and $\partial \underline{v}/\partial x_3$ are calculated simultaneously.

Calculation of $\bar{\boldsymbol{B}}_{ek}$: The k'th mode unimodular elastic left Cauchy-Green strain tensor $\bar{\boldsymbol{B}}_{ek}$ is calculated from (3.8). A variable-order variable-time step backward difference scheme is used to integrate (3.8) over a certain time interval. During each time interval, say $t_n \rightarrow t_{n+1}$, $\boldsymbol{L}$ is assumed to be constant and the initial value of $\bar{\boldsymbol{B}}_{ek}$ is $\bar{\boldsymbol{B}}_{ek}(\vec{s}_n, t_n)$.

6. Example

As an example, polycarbonate (PC) is injected into a cavity of $80 \times 50 \times 2$ mm (length, width, height), see Fig. 2. Along A a line gate is assumed. The material properties of PC in the case where a viscoelastic constitutive model is used are given in Table 1.

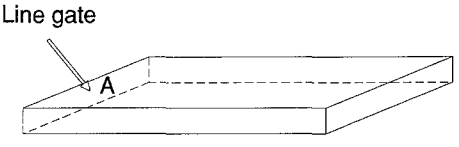

Fig. 2. Sketch of the cavity, strip of 80·50·2 mm

Table 1. Parameters for PC

Parameters WLF equation:				
$T_0 = 200\,°C$				
$C_1 = -4.217$				
$C_2 = 94.95\,°C$				
Thermal properties:				
$c_p = 1.5$	J/gK			
$\lambda = 0.27\ 10^{-3}$	J/s mm K			
Visco-elastic properties:				
$\eta' = 0.003\,\bar{\eta}$	MPas			
$\theta_1 = 10^{-1}$ s		$\eta_1 = 9.74\ 10^{-3}$	MPas	
$\theta_2 = 10^{-2}$ s		$\eta_2 = 6.75\ 10^{-3}$	MPas	
$\theta_3 = 10^{-3}$ s		$\eta_3 = 1.25\ 10^{-3}$	MPas	
$\bar{\theta}_1 = 10^{-10}$ s		$\bar{\eta}_1 = 894\ 10^{-10}$	MPas	
Tait parameters:				
$s = 0.51\,°C/MPa$				
	solid	melt		
$a_0 = 868$		868		mm^3/g
$a_1 = 0.22$		0.577		mm^3/gK
$B_0 = 395.4$		316.1		MPa
$B_1 = 2.609\ 10^{-3}$		$4.078\ 10^{-3}$		$°C^{-1}$

Processing conditions PC: The material is injected at an average velocity of 120 mm/s at 320 °C. This velocity is maintained at A until the holding pressure of 50 MPa is reached. The holding pressure is maintained at A until the elapsed time exceeds 4.0 s. At this time the gate is assumed to freeze off. Clearly, an accurate model of gate freeze off is not available yet, and it is unlikely that the pressure remains at 50 MPa in reality. The proper modeling of the behavior in and near the gate is still an open question. As can be seen from the results later on, the period of time that the gate remains open determines, to a large extent, the amount of residual birefringence in the product. The mold has a temperature of 80 °C.

Results for PC: Calculations are performed with both the viscoelastic and the viscous model. Figure 3 shows the calculated pressure history at $x_1 = 8$ mm and $x_1 = 56$ mm for the viscoelastic case. They virtually coincide with the results of the viscous model, which are not shown. During the filling of the mold, for $t \in [0, t_f = 0.67]$ s, the pressure gradually rises. Then a short compression stage follows where the pressure rapidly increases to 50 MPa. Hereafter, due to cooling, the pressure slowly drops. After solidification of the gate the pressure drops further until the product is ejected from the mold.

Figures 4 to 8 show the evolution of the *first normal stress difference* N_1, defined as $N_1 = \tau^e_{11} - \tau^e_{33}$, for the viscoelastic (direct) case. N_1 is shown at 5 times: at the end of the filling stage $t_f = 0.67$ s, at the end of the compression stage $t_c = 0.71$ s, and at $t = 2.7$, 3.2 and 4.7 s. During the compression stage most of the flow-induced normal stresses relax because the flow rate is low and the temperature at the core of the cavi-

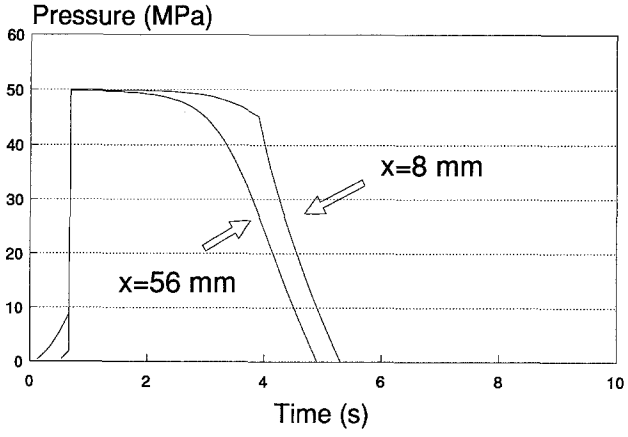

Fig. 3. Numerical pressure trace for PC, viscoelastic material model

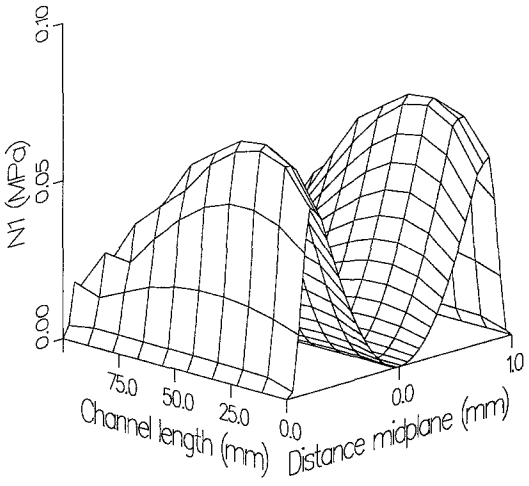

Fig. 4. N_1 at end of filling stage, $t = 0.67$ s

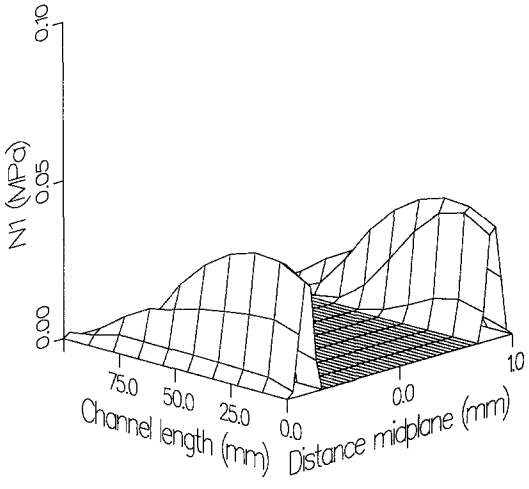

Fig. 5. N_1 at end of compression stage

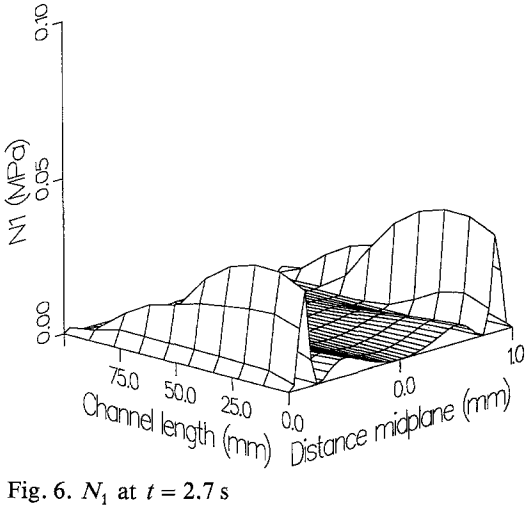

Fig. 6. N_1 at $t = 2.7$ s

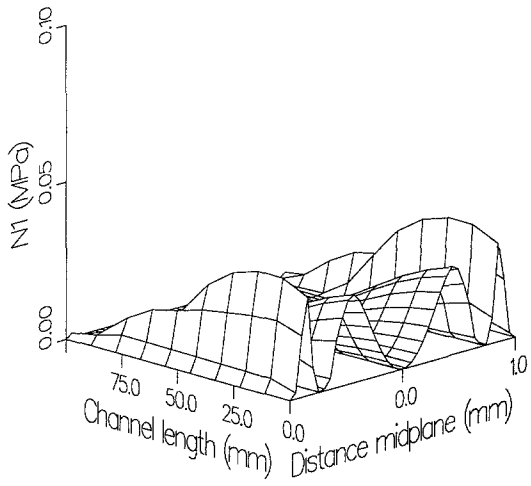

Fig. 7. N_1 at $t = 3.21$ s

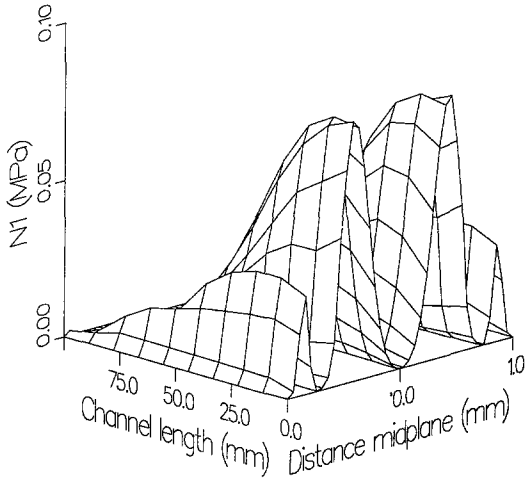

Fig. 8. N_1 at $t = 4.7$ s

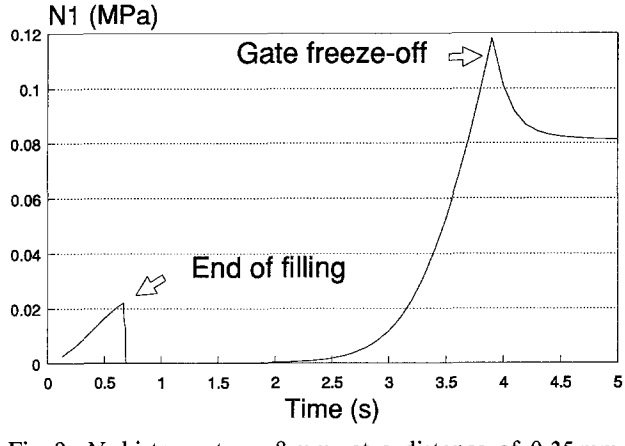

Fig. 9. N_1 history at $x = 8$ mm, at a distance of 0.35 mm from the midplane

ty is still quite high, compare Figs. 4 and 5. This does not apply to regions close to the walls, because there the temperature has dropped below T_g and relaxation has virtually stopped. During the post-filling stage shear rates are several orders of magnitude smaller than in the filling stage. However, due to the decreasing temperature as time proceeds, small shear rates may still introduce considerable normal stresses, as is clearly demonstrated in Figs. 5 to 8. Figure 8 shows the final N_1 distribution because at that time all material has solidified. After about $t = 2.5$ s the first normal stress difference almost explodes to a very high value, indicating that packing times should be limited if minimal residual birefringence is required. This is clearly shown in Fig. 9, which shows the N_1-history at $x = 8$ mm at a distance of 0.35 mm from the midplane.

These results can be compared with calculations obtained with the *indirect* method, where the kinematics of the generalized Newtonian model is used to calculate flow-induced residual stresses with the compressible Leonov model. Figure 10 compares N_1 obtained with both techniques at $x = 8$ mm. Qualitatively, the results are in very good agreement, while the computation time of the indirect method is less than 1/10 of the direct method. This implies that the more cost-effective, indirect, method can be used as an indicator for molecular orientation, and hence as a method to assign anisotropic material properties to the model.

Figures 11 to 19 show the evolution of the thermally-induced σ_{11}. In the final time step the material is forced to cool down to the final uniform temperature of 20 °C. This explains the wide difference between Figs. 18 and 19. Note that the stresses are positive *at* the edge, negative *near* the edge, and positive in the

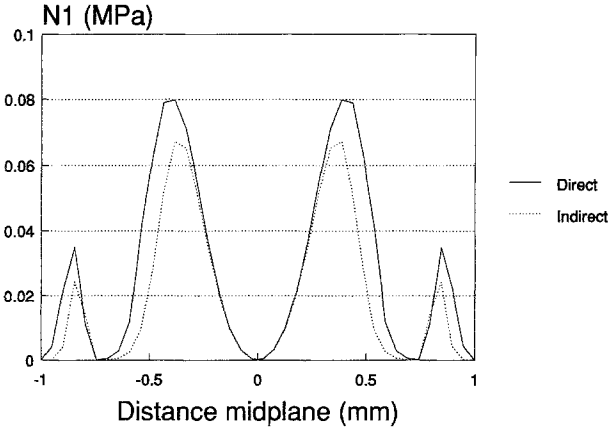

Fig. 10. Comparison of N_1 at $x_1 = 8$ mm

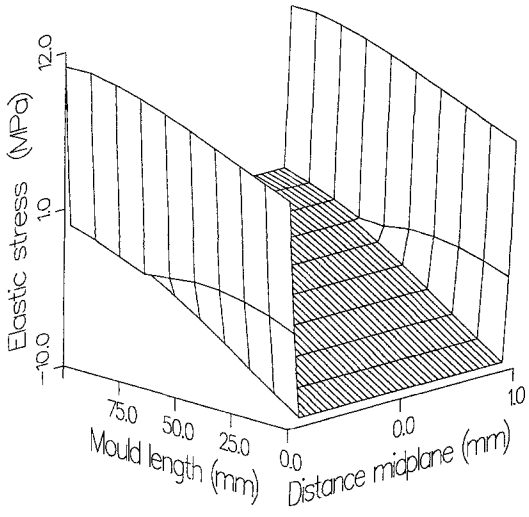

Fig. 11. Thermally induced stress at $t = 0.67$ s

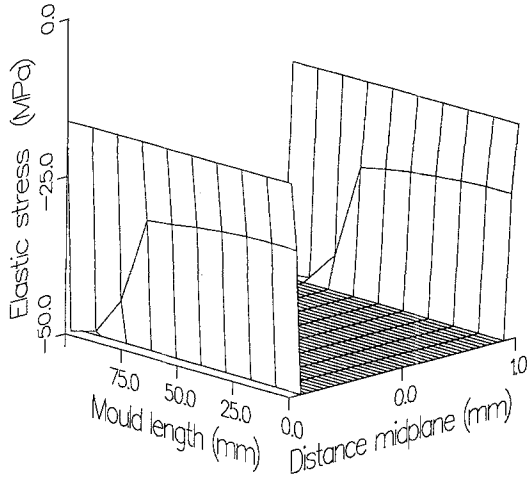

Fig. 12. Thermally induced stress at $t = 0.7$ s

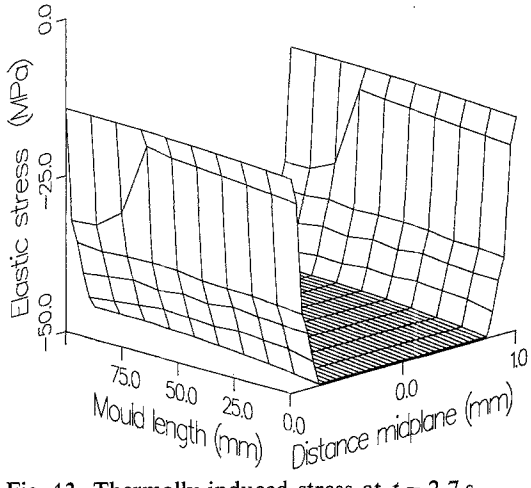

Fig. 13. Thermally induced stress at $t = 2.7$ s

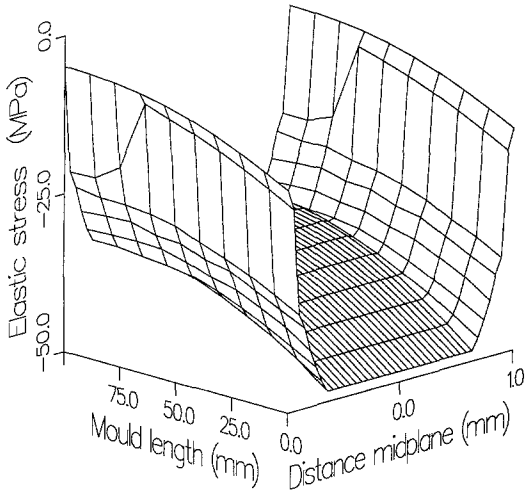

Fig. 14. Thermally induced stress at $t = 3.7$ s

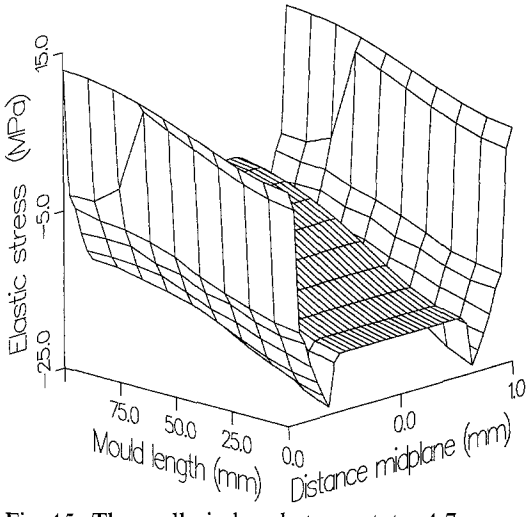

Fig. 15. Thermally induced stress at $t = 4.7$ s

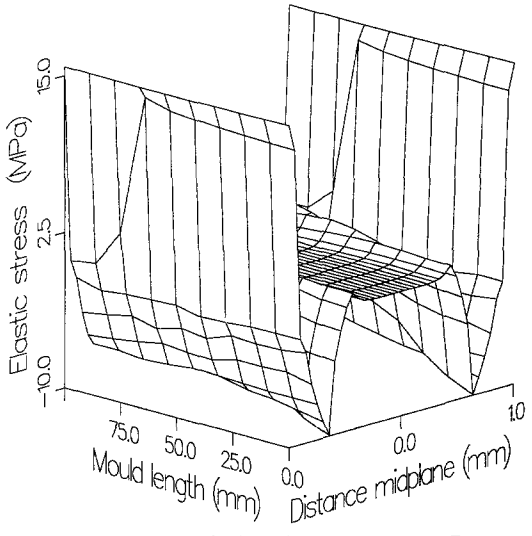

Fig. 16. Thermally induced stress at $t = 5.7$ s

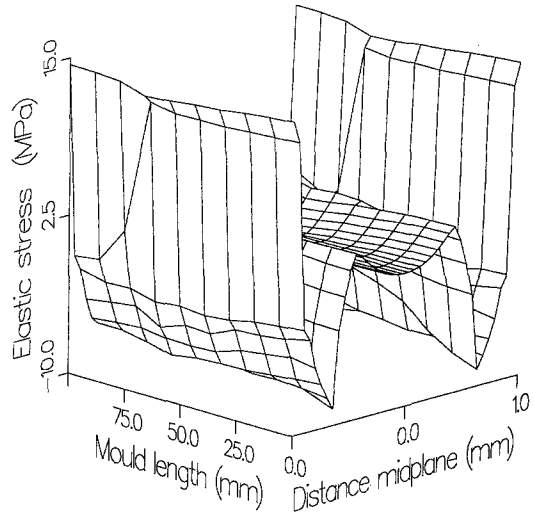

Fig. 17. Thermally induced stress at $t = 6.7$ s

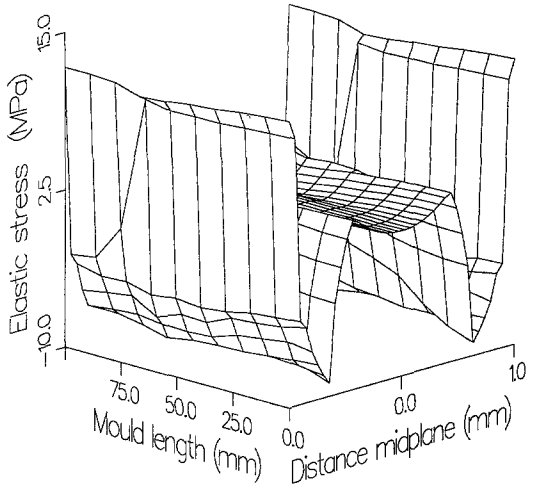

Fig. 18. Thermally induced stress at $t = 7.7$ s

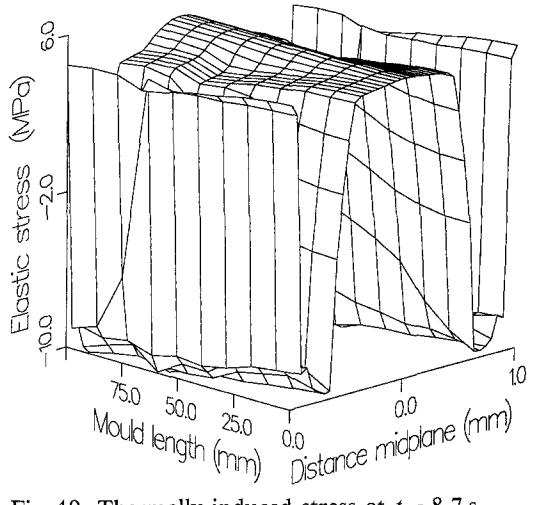

Fig. 19. Thermally induced stress at $t = 8.7$ s

core. This stress distribution is markedly different from what is found in free quench experiments (see Wimberger-Friedl and Hendriks [15]). The difference is due to the pressure evolution in the molten part of the product: solidification takes place at elevated pressures.

The effect of mold elasticity is shown in Fig. 20. The mold elasticity is modeled very crudely by

$$\frac{dh}{dt} = \frac{dh}{dp}\frac{dp}{dt}, \tag{6.1}$$

where $dh/dp = 0.4\ \mu m/MPa$ is chosen. As is seen from Fig. 20, this small amount of mold elasticity has a significant influence on the pressure history in the mold and, therefore, on the final thermally-induced stress state, as shown in Fig. 21. Note, however, that the thermally-induced stress theory does not include mold elasticity, so Fig. 21 must be handled with care. Essentially, assumption 9 of Section 4.3 implies that $\int_{-h_m/2}^{h_m/2} \varepsilon_{33}\, dx_3 = 0$. This assumption must be altered to formally include mold elasticity into the thermally-induced stress theory. The current calculation only includes the effects of the change in pressure history.

Finally, Fig. 22 shows part of the temperature history of a point at $x_1 = 8$ mm at the midplane. It clearly demonstrates the effect of heat due to compression, a phenomenon that is not negligible.

7. Conclusions

The evolution of both flow- and thermally induced stresses during injection molding in both the filling and the post-filling stage is investigated numerically. A compressible version of the Leonov model was developed and applied.

The calculations show clearly that a substantial portion of the flow-induced residual stresses arise during the post-filling stage. This is in agreement with experimental data [13]. The indirect approach gives a good qualitative and a reasonable quantitative prediction of flow-induced residual stresses when compared with the direct, viscoelastic approach. In this indirect method the pressure problem is derived with generalized Newtonian material behavior, and the resulting kinematics is supplied to the viscoelastic constitutive equation. This approach is a valuable tool to give a quick and fairly accurate indication of the molecular orientation in an injection molded product (provided that one assumes that flow-induced stresses are a measure of molecular orientation).

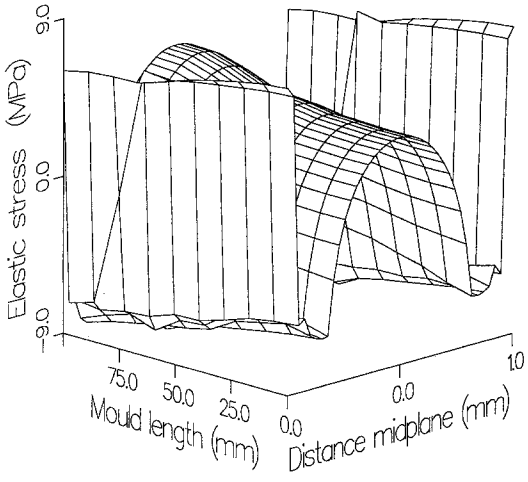

Fig. 21. Thermally induced stress at $t = 8.7$ s in case of mold elasticity

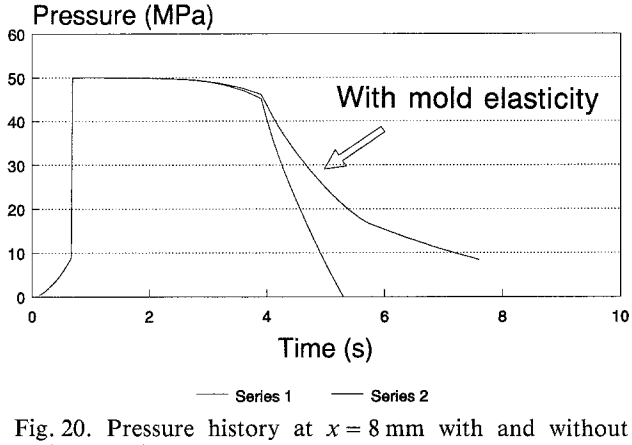

Fig. 20. Pressure history at $x = 8$ mm with and without mold elasticity

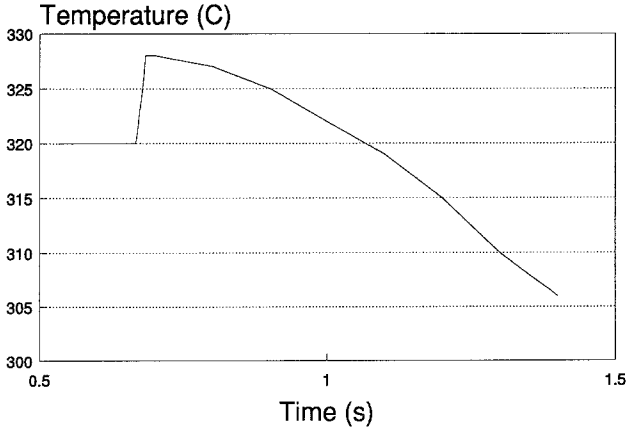

Fig. 22. Effect of heat due to compression

As yet, the effect of the molecular orientation upon the material properties has not been taken into account. This is mainly due to a lack of experimental data. But, indeed, the intention is to use the flow-induced stresses as a measure of orientation such that anisotropic phenomena can be included in the calculation of thermally-induced residual stresses. This is the topic of ongoing investigations.

It is shown that a small amount of mold elasticity has a marked effect on the pressure history in the mold. This is true even though the model of mold elasticity that is applied is very crude. All currently available commercial analysis codes assume a rigid mold. Particularly at locations in the mold along the plane that separates two mold halfs, mold elasticity is a significant phenomenon. It is not uncommon that molded parts are thicker than the initial cavity thickness. Typically, analysis codes tend to underpredict the pressure in the mold at such locations, due to the disregarding of mold elasticity, and henceforth underpredict the product thickness. Therefore, besides as thermal analysis of the mold, a mechanical analysis of the mold is also required. Thus, the entire system, i.e., mold and product, should be analyzed thermomechanically.

Appendix: Derivation of the pressure problem

Substitution of (4.4) into (4.1) gives

$$\nabla p = \frac{\partial}{\partial x_3}\left(\eta' \frac{\partial \underline{v}}{\partial x_3} + \underline{\tau}^e\right), \quad \underline{\tau}^{eT} = [\tau^e_{13}\ \tau^e_{23}] \ . \quad (A.1)$$

Step 1. Integrating (A.1) with respect to x_3 yields (note that $p = p(x_1, x_2)$)

$$\frac{\partial \underline{v}}{\partial x_3} = \frac{1}{\eta'}(x_3 \nabla p + \underline{c} - \underline{\tau}^e) \ , \quad (A.2)$$

where $\underline{c}$ is an integration constant column.

Step 2. The velocity $\underline{v}$ is found by integrating (A.2) from s^- to x_3

$$\underline{v} = \int_{s^-}^{x_3} \frac{\partial \underline{v}}{\partial x_3} dx_3 = \int_{s^-}^{x_3} \frac{1}{\eta'}(x_3 \nabla p + \underline{c} - \underline{\tau}^e)\, dx_3 \ . \quad (A.3)$$

This holds because at $x_3 = s^-$ $\underline{v} = \underline{0}$. Because $\underline{v} = \underline{0}$ at $x_3 = s^+$ as well, it follows that

$$\underline{c} = -\frac{J_1}{J_0}\nabla p + \frac{1}{J_0}\int_{s^-}^{s^+} \frac{\underline{\tau}^e}{\eta'} dx_3 \ . \quad (A.4)$$

Step 3. Integrating the velocity with respect to x_3 once more gives (after repeated use of $\int f g_{,x} dx = fg - \int f_{,x} g\, dx$).

$$\int_{s^-}^{s^+} \underline{v}\, dx_3 = \left(-J_2 + \frac{J_1^2}{J_0}\right)\nabla p - \frac{J_1}{J_0}\int_{s^-}^{s^+} \frac{\underline{\tau}^e}{\eta'} dx_3 + \int_{s^-}^{s^+} \frac{x_3 \underline{\tau}^e}{\eta'} dx_3 \ . \quad (A.5)$$

Step 4. Integration of the continuity relation (4.5) from s^- to s^+, the use of (A.5) and the recognition that

$$\frac{dh}{dt} = \int_{s^-}^{s^+} \frac{\partial v_3}{\partial x_3} dx_3 = v_3(s^+) - v_3(s^-) \quad (A.6)$$

gives the final result.

References

1. Boshouwers G, Werf J v d (1988) Inject-3, a simulation code for the filling stage of the injection moulding process of thermoplastics. Ph D Thesis, Eindhoven Univ Technology
2. Sitters C (1988) Numerical simulation of injection moulding. Ph D Thesis, Eindhoven Univ Technology
3. Manzione LT (1988) Application of Computer Aided Design in injection molding. Hanser Publ, NY, USA
4. Isayev AI, Hieber CA (1980) Toward a viscoelastic modeling of the injection molding of polymers. Rheol Acta 19:168 – 182
5. Leonov AI (1976) Nonequilibrium thermodynamics and rheology of viscoelastic polymer media. Rheol Acta 15:85 – 98
6. Stickforth J (1986) The rational mechanics and thermodynamics of polymeric fluids based upon the concept of a variable reference state. Rheol Acta 25:447 – 458
7. Simo JC (1987) On a fully three dimensional finite strain viscoelastic damage model: formulation and computational aspects. Comp Meth Appl Mech Eng 60:153 – 173
8. Upadyay RK, Isayev AI, Shen SF (1981) Transient shear flow behaviour according to the Leonov model. Rheol Acta 20:443 – 457
9. Leonov AI (1987) On a class of constitutive equations for viscoelastic liquids. J Non-Newtonian Fluid Mech 15:1 – 59
10. Zoller PA (1982) A study of the pressure-volume-temperature relationships of four related amorphous polymers: polycarbonate, polyarylate, phenoxy and polysulfone. Polym Sci 20:1453 – 1464
11. Pironneau O (1982) On the transport-diffusion

algorithm and its application to the Navier-Stokes equation. Numer. Math 38:309 – 332
12. Morton KW, Priestly A, Suli E (1986) Stability analysis of the Lagrange-Galerkin method with non-exact integration. Oxford University Computing Laboratory, Report 86/14
13. Wimberger-Friedl R, Janeschitz-Kriegl H (1989) Residual birefringence in Compact Discs, submitted for publication
14. Hughes TJR (1987) The finite element method. Prentice-Hall International Editions, Englewood Cliffs, New Jersey
15. Wimberger-Friedl R, Hendriks RDHM (1989) The measurement and calculation of birefringence in quenched polycarbonate specimens. Polymer 30:1143 – 1149

(Received September 9, 1990; accepted September 13, 1990)

Authors' address:

Prof. dr. ir. F.P.T. Baaijens
Philips Research Laboratories
P.O. Box 80000
5600 JA Eindhoven
The Netherlands